C. R. Geoscience 350 (2018) 89–99

Contents lists available at ScienceDirect

Comptes Rendus Geoscience

www.sciencedirect.com

Petrology, Geochemistry

Petrogenesis of the Mairupt microgranite: A witness of an Uppermost Silurian magmatism in the Rocroi Inlier, Ardenne Allochton

Corentin Cobert [a,*], Jean-Marc Baele [a], Philippe Boulvais [b], Marc Poujol [b], Sophie Decrée [c]

[a] Geology and Applied Geology, University of Mons, 9, rue de Houdain, 7000 Mons, Belgium
[b] Université Rennes, CNRS, Géosciences Rennes, UMR 6118, 35000 Rennes, France
[c] Royal Belgian Institute of Natural Sciences, Brussels, Belgium

ARTICLE INFO

Article history:
Received 5 December 2017
Accepted after revision 30 December 2017
Available online 27 February 2018
Handled by Marc Chaussidon

Keywords:
Microgranite
LA–ICP–MS U–Pb dating
Silurian magmatism
Rocroi inlier
Ardenne

ABSTRACT

Magmatism in the Rocroi inlier (Ardenne Allochton, southeastern Avalonia during eo-Hercynian times) consists of a swarm of bimodal dykes (diabase and/or microgranite) emplaced in Middle to Upper Cambrian siliciclastics (Revin Group). Felsic volcanites interbedded within the Upper Silurian/Lower Devonian transgressive strata on the eastern edge of the inlier were interpreted as belonging to the same magmatic event. This was subsequently invalidated by zircon U–Pb dating of the Mairupt and Grande Commune magmatic rocks, which yielded an Upper Devonian age. Here we report a reevaluation of the age of the Mairupt microgranite based on LA–ICP–MS in situ U–Pb zircon geochronology, which yields a concordant age of 420.5 ± 2.9 Ma (Late Silurian/Early Devonian). This new dating restores the consistency between the different magmatic occurrences in the Rocroi inlier. The geochemical and petrographical data furthermore indicate a major crustal contribution, which fits well within the context of crust thinning of the Ardenne margin (southeastern Avalonia) in the transtensional Rheno-Hercynian back-arc basin.

1. Introduction

The Rocroi inlier belongs to the Ardenne Allochton, which, at the scale of the Hercynian belt, corresponded to the southeastern part of Avalonia. In the southern part of the inlier, the magmatism is mainly represented by tholeiitic dykes forming an ENE–WSW-elongated, 20×8 km swarm (André, 1983; Fig. 1). According to Goffette (1991), 80% of the 144 known dykes are mafic (diabase) and 20% are felsic (microgranite). Felsic dykes are more abundant to the east where some microgranite occurrences show diabase enclaves and linings on dyke walls, witnesses of an older mafic intrusion. In Willerzie, located on the northeastern edge of the Rocroi inlier (Fig. 1), Upper Silurian to Lower Devonian sediments of the Haybes Fm. have been intersected by the Willerzie borehole (Meilliez, 2006; Roche et al., 1986). They contain rhyolitic clasts and abundant quartz phenocrysts indicative of a volcano-sedimentary origin. Similar quartz-rich rocks (porphyroids) outcropping in the Willerzie area were interpreted as being related to the same magmatic event, which produced the dyke swarm in the southern Rocroi inlier (Beugnies, 1969; Beugnies and Charlet, 1970). This

* Corresponding author.
E-mail address: corentin.cobert@umons.ac.be (C. Cobert).

https://doi.org/10.1016/j.crte.2017.12.001
1631-0713/

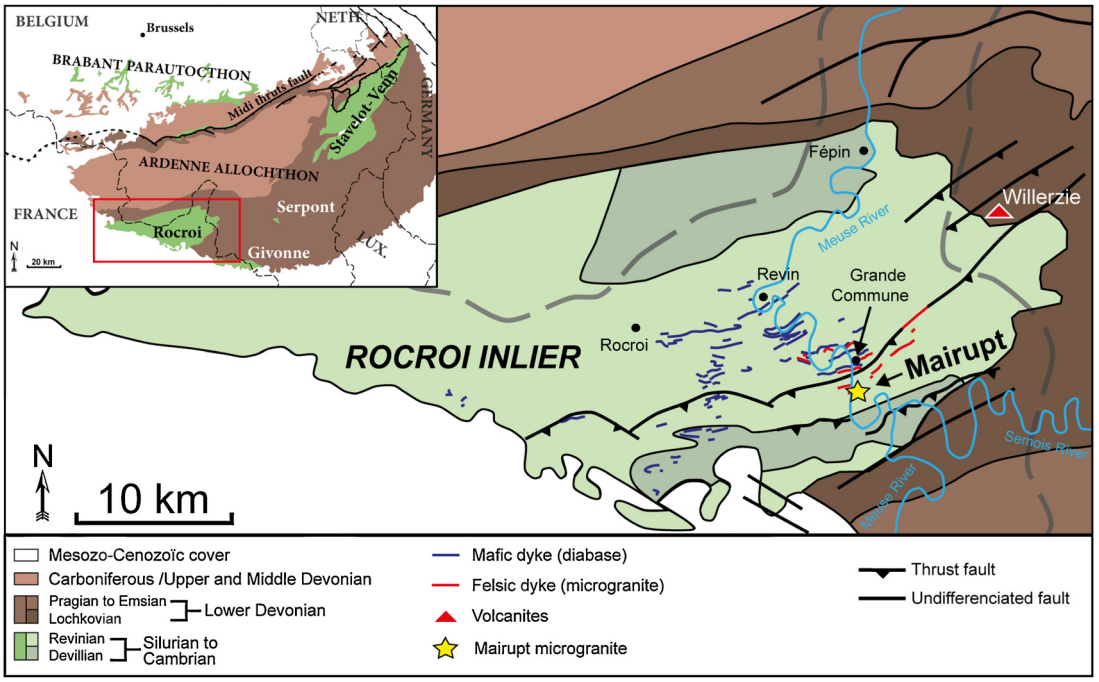

Fig. 1. Simplified geological map of the Rocroi inlier with location of the study area and the dyke swarm (after Beugnies, 1963 and Goffette, 1991).

was later invalidated by Goffette et al. (1991), based on ID-TIMS dating of zircon concentrates from the Grande Commune diabase and the Mairupt microgranite, which yielded a Late Devonian lower intercept age of 373 +8/–9 Ma. The magma was therefore interpreted as being emplaced during the Variscan maximum extensional event.

Furthermore, if the mafic dykes are clearly related to the melting of the lithospheric or asthenospheric mantle, there is, to date, no clear indication of the origin of the felsic dykes (differentiation from a mafic magma or crust melting). Therefore, investigating the petrogenesis of the Mairupt microgranite, considered as the felsic end-member of the Rocroi magmatism, is the second objective of this study, which was conducted on the same samples that were used for dating. The Mairupt microgranite was chosen because it was previously studied (e.g., Goffette et al., 1991) and is easily accessible for field study and sampling.

In this paper, we report new geochronological data for the Rocroi inlier magmatism within a brief petrographical and geochemical framework. The latter aims to decipher the source of the magmatic rocks and the context prevailing at the time of their emplacement.

2. Geological setting

The Ardenne Allochthon is part of the Variscan fold and thrust belt. It is bounded to the north by the Midi thrust fault and, to the south, by the Meso-Cenozoic cover of the Paris basin (Fig. 1; insert). The Ardenne Allochthon is essentially composed of Upper Silurian and Devono-Carboniferous sediments, several kilometers thick, with Upper Silurian and Lower Devonian siliciclastics and Upper Devonian/Carboniferous mixed carbonate–siliciclastics. The Upper Silurian and Devono-Carboniferous series unconformably overlie Lower Paleozoic rocks, which are mainly composed of Cambrian to Ordovician mudstones and sandstones or metapelites and quartzites, their metamorphic equivalent. Lower Paleozoic rocks occur in several inliers: Rocroi, Stavelot-Venn, Givonne, and Serpont.

The Rocroi inlier is an ENE–WSW 20 × 70 km elongated antiform (Fig. 1). It is constituted of a ~2km-thick metapelitic and quartzitic sedimentary pile, predominantly Cambrian in age. Two main lithostratigraphic units are distinguished: the Deville and the Revin Groups (Beugnies, 1968; Gosselet, 1888; Lacquement, 2001; Meilliez, 1989). The sediments of the Deville Group (Lower Cambrian, about 400 to 600 m thick) have a rather light color and were deposited in a shallow platform environment as sandstone and siltstone formations. The sediments of the Revin Group (Middle to Upper Cambrian and Lower Ordovician, > 1000 m thick) are dominated by dark mudstones and siltstones that were deposited in a deeper environment, with common turbiditic sequences. The Mairupt microgranite is intrusive into the middle Revin Group, which is composed of dark, pyritic, and psammitic metapelites and quartzites.

The overall structure of the eastern half of the Rocroi inlier may be summarized as a wide syncline in its central part (Revin Group) bounded by two anticlines (Deville Group). Folds are east–west-trending, north-verging, and sometimes overturned. Cleavage is dipping to the south in both the Lower Paleozoic rocks from the inlier and the unconformably overlying Upper Silurian/Devono-Carboniferous formations.

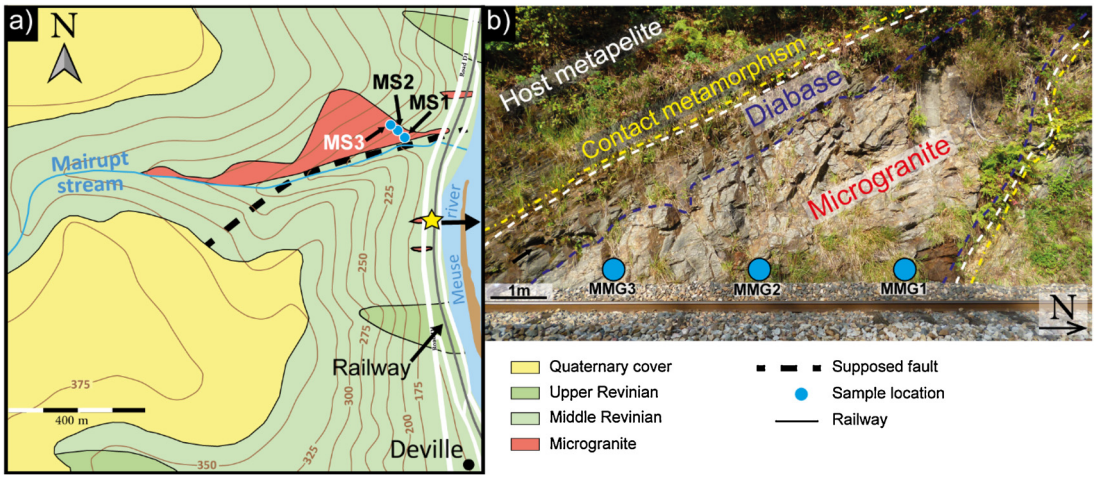

Fig. 2. (a) Detailed geological map of the Mairupt area (after the 1:50,000 French geological map of Fumay) and (b) section of the railway outcrop of Mairupt, which is shown by the yellow star on the map (a). Blue circles indicate sampling locations in the north stream (a) and railway sites (b) respectively.

3. Field descriptions

The Mairupt microgranite is located in the Revin group exposed along the Meuse valley in the southeastern part of the Rocroi inlier (Fig. 1). Several microgranite outcrops are found to the north of the Mairupt stream (Fig. 2a) and along the railway parallel to the Meuse River (Fig. 2b).

To the north of the Mairupt stream, there are several large microgranite outcrops, but the geometry of the magmatic body cannot be constrained since the host rock is not exposed. The geological map (Fig. 2a) suggests an irregular microgranite mass, which is thinning westwards.

To the south of the Mairupt stream, an up to 4 m-thick microgranite body is well-exposed in a north–south section along the railway (Fig. 2b). In this section, both the upper and lower boundaries of the magmatic rock are visible and define a lenticular morphology.

The microgranite body is fairly homogeneous, except on its outer rims, where it is flanked by a dark, fine-grained rock (diabase), which is about 1 m and 0.2 m thick on its southern and northern sides, respectively. The contacts between the diabase and the microgranite are gradual over a few millimeters, and a few diabase enclaves occur within the microgranite. This indicates that the felsic intrusion closely followed the mafic intrusion, as it is the case for other similar mixed diabase/microgranite dykes that are known in the Rocroi inlier (Goffette, 1991).

This dyke is intrusive within the metapelitic host rock, which exhibits a decimeter-thick brownish zone along the contact with the microgranite. This zone is interpreted as a contact metamorphism zone.

The regional cleavage in the Cambrian metasediments, which strikes east–west and dips 30° towards the south, is draping the microgranite. The microgranite thus appears as a decameter-scale boudin isolated within the Cambrian metasediments. The microgranite body to the north of the Mairupt stream may thus be the result of the boudinage of an initially more continuous microgranitic intrusion (dyke or sill). Clearly, the microgranite was emplaced in the host rock before the Variscan deformation, which is consistent with the observed deformation within the microgranite (Fig. 3, see below).

In the host metasediments, folded and boudinaged quartzite layers occur in the globally pelitic formation. Cleavage is mainly parallel to stratification. Shear bands are visible to the south of the microgranite body. They are sub-horizontal and cleavage becomes parallel to the shear bands in their vicinity. These shear bands appear as C' bands and cleavage-shearing relationships indicate a top-to-the-north displacement, thus an apparent thrusting with a northward vergence. At a regional scale, this deformation is consistent with the Variscan thickening accommodated by large-scale folds with ENE–WSW axes and thrusts that are common in the Ardenne Allochthon (Fig. 1).

4. Materials and methods

4.1. Sampling

Sampling of the microgranite bodies was conducted both to the north of the Mairupt stream (MS1, 2 and 3; Fig. 2a) and along the railway (MMG1, 2 and 3; Fig. 2b). These six samples cover the petrographic variability observed in the microgranite, which is mainly due to a variation in the abundance of the large K-feldspar phenocrysts (Fig. 3, see below). The diabase flanking the microgranite was not sampled. In total, 12 microgranite thin-sections were prepared.

4.2. Microscopy

The polished microgranite thin-sections were studied under optical, cathodoluminescence and electron microscopy. Cathodoluminescence was performed at UMONS using a CITL (Cambridge Image Technology Ltd) Mk5 cold-cathode CL unit operated at 15 kV and 500 μA acceleration voltage and beam current, respectively. This technique was used to quickly locate and characterize zircon crystals for further in situ LA–ICP–MS dating. A Quanta 20 ESEM (FEI)

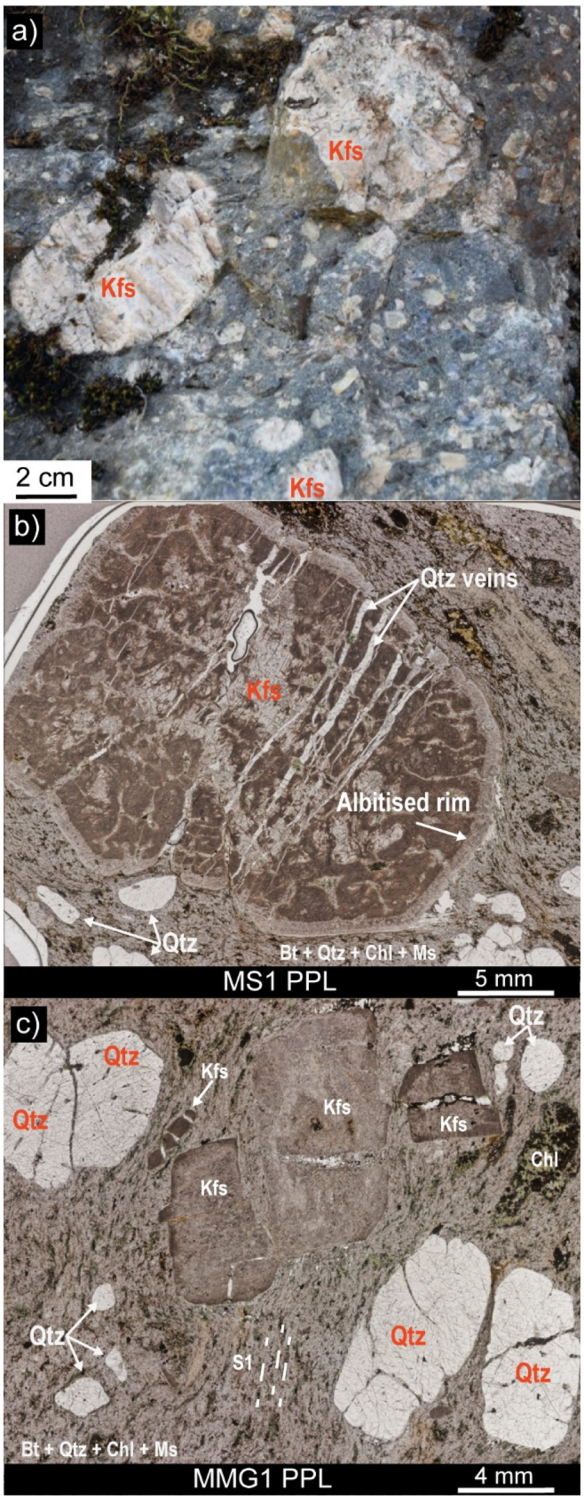

Fig. 3. (a) Macroscopic and (b,c) microscopic pictures of the Mairupt microgranite. (a) Porphyritic texture of the microgranite with K-feldspar phenocrysts in a microcrystalline groundmass. (b) Plane-polarized light micrograph of a K-feldspar phenocryst showing boudinage, albitization and the draping cleavage. (c) Plane-polarized light micrograph of MMG1 microgranite sample showing rounded quartz grain, boudinaged K-feldspar and chloritization. Qtz: Quartz; Kfs: K-feldspar; Pl: plagioclase; Bt: biotite; Ms: muscovite; Chl: chlorite.

Scanning Electron Microscope (SEM) with energy-dispersive spectroscopy (EDS; Apollo 10 Silicon Drift detector) was used for electron microscopy at the Royal Belgian Institute of Natural Sciences.

4.3. Major and trace elements

The microgranite samples were crushed following a standard protocol to obtain a powder using agate mortars. Chemical analyses were performed by the "Service d'analyse des roches et des minéraux" (SARM; CRPG-CNRS, Nancy, France) using ICP-AES for major elements and ICP–MS for trace elements following the techniques described in Carignan et al. (2001).

4.4. LA–ICP–MS U–Pb dating

The U–Pb geochronology of zircon grains was conducted in context, directly in thin sections by in situ Laser Ablation–Inductively Coupled Plasma–Mass Spectrometry (LA–ICP–MS) at Géosciences Rennes using an ESI NWR193UC Excimer laser coupled with a quadrupole Agilent 7700x ICP–MS. During the course of an analysis, the signals of ^{204}(Pb + Hg), ^{206}Pb, ^{207}Pb, ^{208}Pb, ^{232}Th, and ^{238}U masses are acquired. No common Pb correction was applied owing to the large isobaric interference with Hg. The ^{235}U signal is calculated from ^{238}U based on the ratio ^{238}U/^{235}U = 137.88. Single analyses consisted of 20 s of background integration followed by 60 s of integration with the laser firing and then a 10 s delay to wash out the previous sample. For more information on the settings of the instruments, see Supplementary Table 1 and Ballouard et al. (2015). Spots diameters of 20 and 30 μm, a repetition rate of 3 Hz and a laser fluence of 8 J·cm^{-2} were used during this study. The data were corrected for U–Pb and Th–Pb fractionation and for the mass bias by standard bracketing with repeated measurements of the GJ1 zircon standard (Jackson et al., 2004). Repeated analyses of the Plešovice zircon standard treated as unknown (337.4 ± 2.9 Ma, MSWD = 0.19; n = 8); TIMS age ca 337 Ma; Sláma et al., 2008) were used to control the reproducibility and accuracy of the corrections. Data reduction was carried out with the GLITTER® software package developed by the Macquarie Research Ltd. (Van Achterbergh et al., 2001). Concordia diagrams were generated using Isoplot/Ex (Ludwig, 2001). All errors given are listed at one sigma, but where data are combined to calculate an age, the final results are provided with 95% confidence limits.

4.5. Sr and Nd analyses

Sr and Nd isotope analyses were performed on 100-mg powdered samples at Géosciences Rennes, using a 7-collector Finningan MAT-262 mass spectrometer. Rock powders were dissolved with a mixture of 2/3 HF + 1/3 HNO_3 in a sealed Savilex beaker on a hot plate during 3–4 days. They were then dried and taken up with concentrated HCl. Sm, and Nd concentrations were determined by isotope dilution using a ^{149}Sm/^{150}Nd spike. All samples were spiked before dissolution. During the analytical session, measurements of the AMES Nd standard gave a

mean $^{143}Nd/^{144}Nd$ ratio of 0.511980 ± 2 ($n = 5$), so that data were normalized to the value of $^{143}Nd/^{144}Nd = 0.511963$. Analyses of the NBS-987 Sr standard yielded a mean $^{87}Sr/^{86}Sr$ ratio of 0.710167 ± 6 ($n = 3$). Consequently, data have been normalized to the reference value of 0.710250. Blanks values for Nd and Sr were < 300 pg and therefore no further corrections were made.

4.6. Petrography

The Mairupt microgranite displays a spectacular porphyritic microgranular texture (Fig. 3). Phenocrysts are quartz, K-feldspar, and plagioclase (Supplementary Table 2). K-feldspar phenocrysts can reach up to 10 cm in size. Quartz phenocrysts have a greyish-blueish color in the hand sample. They are embayed, a feature which is quite common in felsic magmas emplaced close to the surface. The long axis of the phenocrysts is oriented parallel to the cleavage, which drapes the grains (Fig. 3). K-feldspar crystals were affected by boudinage (Fig. 3c). The groundmass is made of quartz, feldspar, biotite, muscovite, and minor amounts of apatite, titanite, and oxides. The microgranite has a higher amount of Fe–Ti oxides along the railway than to the north of the Mairupt stream. Conversely, the groundmass contains a much higher proportion of quartz grains in the Mairupt stream than along the railway.

Regarding alteration, the two selected sampling sites display distinct features. Along the railway, a secondary assemblage of chlorite, calcite, albite, epidote, and opaque minerals develops locally in the groundmass and is best expressed in pressure shadows associated with phenocrysts and in veins cutting large feldspar grains (corresponding to small-scale inter-boudins). Therefore, this secondary assemblage, which is typical of greenschist facies, developed during deformation. In sample MMG1, a vein containing this assemblage is visible, and the quartz phenocrysts in contact with the vein display spectacular dissolution features. To the north of the Mairupt stream, this chlorite + calcite alteration is locally present, but less developed than along the railway. The most prominent feature in this microgranite is the development of secondary quartz micro-crystals, which is typical of secondary silicification. Where this silicification developed around phenocrysts, it is draped by cleavage. Thus, silicification occurred prior to regional deformation.

5. Results

5.1. Major elements

The microgranite samples exhibit variable SiO_2 contents, ranging from 66.7 to 77.6 wt.% (Supplementary Table 3). Samples with the highest SiO_2 contents (MS2 and MS3) show secondary silicification, while the lowest SiO_2 contents are observed in samples with petrographic evidence of greenschist alteration associated with quartz dissolution (MMG1 and MMG3). In the diagram of Hughes (1973), the samples define a horizontal trend towards the low K_2O–high Na_2O side, outside the field of primary igneous rocks (Fig. 4a). Na_2O (3.7 to 6.6 wt.%) and K_2O (0.2 to 2.8 wt.%) are consistently highly variable. Fe_2O_3 and TiO_2 are correlated, the higher contents being found in the samples collected along the railway. The carbonated sample MMG1 is characterized by LOI and CaO contents of 3.2 and 2.3 wt.%, respectively. Overall, the investigated samples have a peraluminous signature (Fig. 4b), the observed dispersion in the diagram being likely due to alteration (this point is discussed below). Although the microgranite is partly albitized, and hence has gained extra Na_2O, the non-silicified samples still plot closer to the tholeiitic trend than the alkaline one in the ($K_2O + Na_2O$) as a function of SiO_2 diagram ($Na_2O + K_2O = 5.2$ to 6.5 wt.%; $SiO_2 = 66.7$ to 70.5 wt.%). This is consistent with André (1983), who distinguished the entire Ardenne area as a tholeiitic province.

5.2. Trace elements

Trace element contents are variable among the six samples (Fig. 5). In the spidergrams, the trace elements that show the highest variability are Rb, Ba, Pb, Sr, which fluctuates consistently with K_2O and Na_2O. Light Rare Earth Elements (LREE), Th, Zr and Hf are less abundant in samples MS2 and MS3, which exhibit the highest SiO_2 content. Interestingly, these samples also display intra-REE fractionation, with patterns showing some tetrad effect (Fig. 5) and a well-developed Eu negative anomaly (Eu/Eu^* down to 0.3). Also, the ratios of twin elements Zr/Hf (24.7 and 27.2) and Nb/Ta (5.4 and 5.9) are different in these samples when compared to the others (Zr/Hf = 33.0–35.8; Nb/Ta = 9.6–10.5). Finally, the silicified samples also have the highest U, W, and Ta contents (Fig. 5).

5.3. Sr and Nd isotopes

The initial $^{87}Sr/^{86}Sr$ isotopic ratios (calculated at 420 Ma, see LA–ICP–MS dating) show large variations, ranging from 0.7116 to 0.7161 (Fig. 6), the lowest value being recorded in sample MS1, which falls in the field of unaltered igneous rocks (Fig. 4a). In contrast, a narrower range of initial $^{143}Nd/^{144}Nd$ values (calculated at 420 Ma) is observed and corresponds to negative $\varepsilon_{Nd(t)}$ varying from -3.8 to -6.3 (Fig. 6; Supplementary Table 4).

5.4. U–Pb LA–ICP–MS dating

In situ dating was performed in context in thin sections on the six samples described above. Under cathodoluminescence, zircon crystals exhibit a typical growth zoning and commonly contain an inner core with irregular sector zoning and/or resorption pattern (Fig. 7c).

For samples from the railway (Supplementary Table 5), 25 analyses were performed on 16 zircon grains. Pb (13.6 to 159.3 ppm) and U (124.7 to 1479 ppm) contents as well as Th/U ratios (0.06 to 1.44) are highly variable. Except for three analyses (Zr6, Zr15a and Zr16; Supplementary Table 5), all the data plot in a concordant to subconcordant position (Fig. 7a). The 13 most concordant data (in bold/highlighted in green in Supplementary Table 5) yield a Concordia age (as of Ludwig, 1998) of

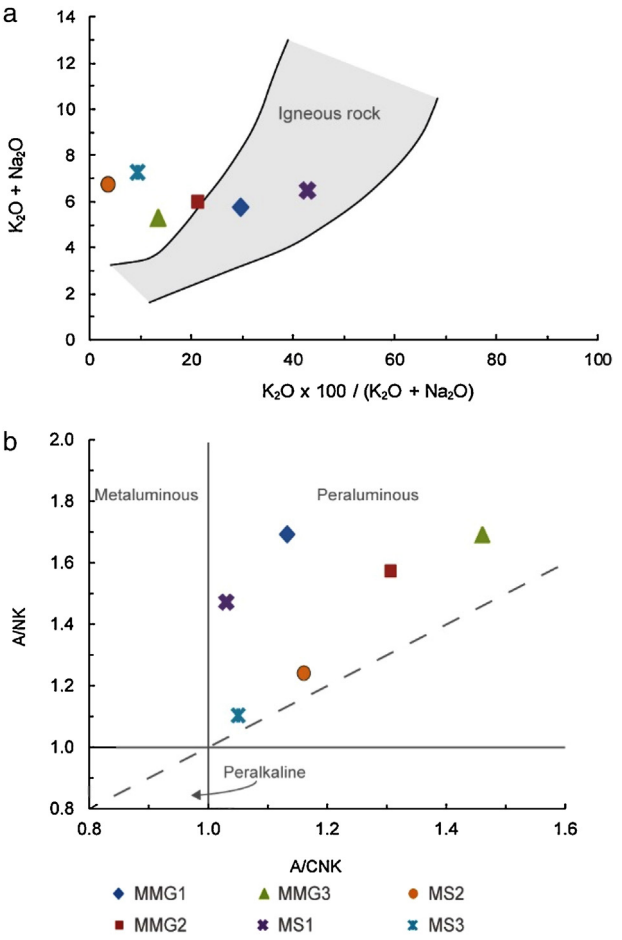

Fig. 4. (a) Hughes (1973) diagram for the Mairupt microgranite. The grey field represents unaltered igneous rocks as defined by Hughes (1973). Out of this field, igneous rocks are altered by albitization (to the left) or potassic alteration (to the right). (b) Shand (1943) diagram for the Mairupt microgranite. A/NK = molar $Al_2O_3/(Na_2O + K_2O)$; A/CNK = molar $Al_2O_3/(CaO + Na_2O + K_2O)$.

420.5 ± 2.9 Ma (MSWD = 0.84; Fig. 7a inset). This date is confirmed by the weighted mean $^{206}Pb/^{238}U$ date of 420.5 ± 2.4 Ma (MSWD = 0.84, probability = 0.64; Fig. 7a and in bold in Supplementary Table 5). The very discordant data Zr6 and Zr16 define older apparent dates, while the position of the remaining data (including Zr15a) can be attributed to various degrees of Pb loss.

For samples collected north of the stream (Supplementary Table 6), 17 analyses on a total of 11 zircon grains were performed. Here again, Pb (5.8 to 1421.3 ppm) and U (49.2 to 1558.9 ppm) contents as well as Th/U ratios (0.01 to 1.06) are highly variable. Thirteen analyses (in bold in Supplementary Table 6) plot in a concordant to sub-concordant position and define a weighted mean $^{206}Pb/^{238}U$ date of 419.9 ± 3.5 Ma (MSWD = 1.2, probability = 0.26; Fig. 7b). The 11 most concordant data (in bold/highlighted in green in Supplementary Table 6) define a Concordia age of 421.1 ± 4.0 Ma (MSWD = 1.7; Fig. 7b inset). Analyses Zr10b&c, which were acquired in a core, display older slightly discordant dates at ca. 800 Ma, while the rim yields a concordant date of 420 ± 4.9 Ma (Fig. 7c). Two older apparent $^{207}Pb/^{206}Pb$ dates (ca. 2700 Ma; Supplementary Table 6) are also observed in analyses Zr8a&b from a single zircon crystal found within a plagioclase phenocryst.

6. Discussion

6.1. Age of magmatism

The two groups of investigated samples yield two well-defined Concordia ages of 420.5 ± 2.9 Ma and 421.1 ± 4.0 Ma. No younger ages were found. As these dates are equivalent within error, we conclude that the Mairupt microgranite emplacement and the associated magmatism in the Rocroi inlier took place ca. 420 Ma ago. In such scenario, the older dates found in zircon cores are interpreted as inherited from either the source of the magma or from the host rock during the ascent or the emplacement of the microgranite body.

This new 420 Ma age (Late Silurian/Early Devonian) differs significantly from the 373 Ma age (Late Devonian) obtained by Goffette et al. (1991) by ID-TIMS on zircon fractions. As demonstrated by the CL imaging, the zircon grains in the Mairupt microgranite can be fairly complex with the presence of inherited cores. Therefore, the dissolution of several grains together to perform ID-TIMS

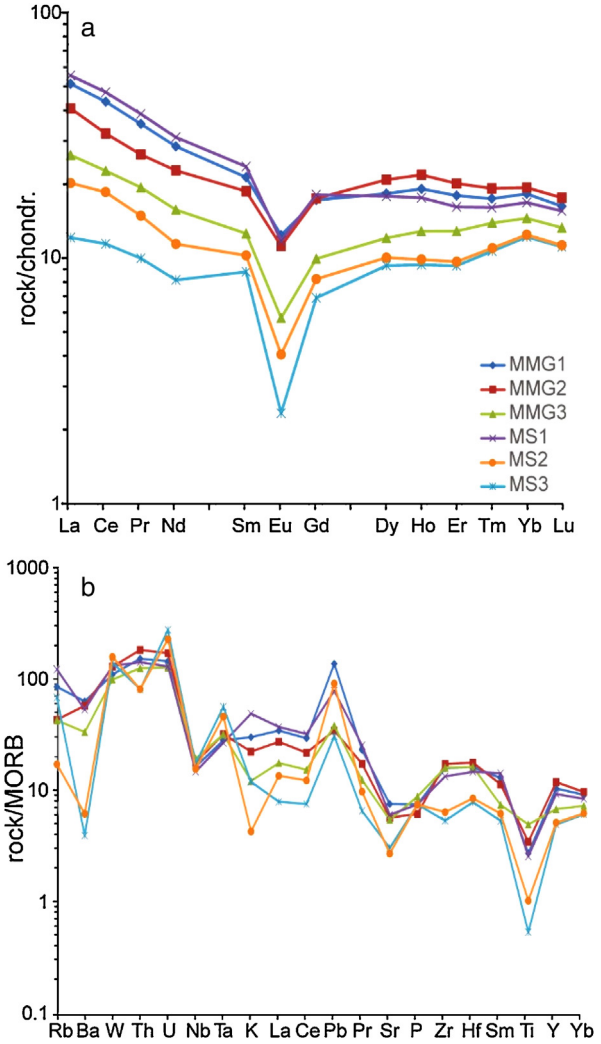

Fig. 5. Trace-element diagrams of the Mairupt microgranite. (a) Chondrite-normalized REE patterns (chondrites values from Evensen et al., 1978). (b) Spidergrams (normalized to MORB; Sun, 1980).

dating can lead to the measurement of mixed, meaningless, apparent ages. Furthermore, the 373 Ma age in Goffette et al. (1991) was defined by only 3 of the 7 fractions analyzed, the last 4 plotting in very scattered positions in the Concordia diagram. Overall, none of these 7 fractions are concordant, and the 373 Ma age corresponds to a lower intercept age (the Discordia returning a Meso-Archean upper intercept age). Our new age is defined by 24 concordant analyses obtained from two different sample sets that were investigated by in situ LA–ICP-MS analysis.

We are therefore confident that the 420.5 ± 2.9 Ma and 421.1 ± 4.0 Ma ages (i.e. Late Silurian/Early Devonian) obtained for the Mairupt microgranite in this study are more robust.

6.2. Petrogenesis

The petrographic description has revealed that the samples have undergone alteration. It thus seems necessary to evaluate the potential effects of these alterations on the geochemistry of these rocks before discussing the petrogenesis of the microgranite.

6.2.1. Effects of secondary alteration

Two types of alteration were recognized in some of the microgranite samples. The first type corresponds to a silicification and developed prior to the regional deformation. The second type is a greenschist facies alteration, marked by chloritization and carbonation, the latter being particularly well expressed in sample MMG1.

Along the railway, the less altered sample is MMG2, and the most altered is MMG1. Note here that sample MMG3 is more mafic, with higher Fe_2O_3 and TiO_2 contents, which likely reflect a slightly distinct magmatic composition, possibly due to the influence of the diabase flanking the microgranite. Noteworthy, the REE patterns of samples MMG1 and MMG2 are somewhat different, sample MMG1 being enriched in LREE and depleted in HREE. This kind of change in the REE distribution likely relates to the presence (or absence) of minor mineral phases controlling the distributions of the LREE (like monazite) or the HREE (like xenotime or zircon). For example, the HREE-rich sample MMG2 is enriched in Th and Zr, which is likely the sign of the presence of a greater amount of zircon grains. It seems then that some geochemical variations did exist before alteration, precluding to propose MMG2 as the protolith of the altered sample MMG1; thus, the establishment of an isocon diagram following Grant (1986) method to characterize element mobilities is not appropriate.

Sample MS1, collected to the north of the stream, could constitute a good protolith to which altered samples could be compared, as this sample falls within the field of unaltered igneous rocks (Fig. 4a). The two other samples in this site are altered to variable degrees. Together with an enrichment in SiO_2, these samples are enriched in Na_2O, U, W, Nb and Ta, depleted in Fe_2O_3, MgO, CaO, K_2O, and present Nb/Ta ratios close to 5. All these variations can be reconciled in a magmatic-hydrothermal process typical of highly evolved melts, implying superimposed silicification and albitization together with extreme magmatic fractionation of minerals that crystallized early during magmatic evolution (like biotite and zircon, for example). Elements such as W, U, Nb behave incompatibly during these processes and are enriched in the fluid-rich evolved melts. The fact that fractionation of elements with comparable charge and radius existed (Zr/Hf and Nb/Ta are fractionated, a tetrad effect is visible in REE patterns) is consistent with the involvement of magmatic-derived fluids (Ballouard et al., 2016). One may question why this process is recorded in the microgranite body to the north of the stream and not in the one found along the railway. The simplest explanation might lie in the fact that the body to the north of the stream is much larger than the other one, allowing internal differentiation processes to occur. The two evolved and altered samples have higher $^{87}Sr/^{86}Sr$ initial ratios than sample MS1. Such an increase in the Sr isotope composition might be due to the incorporation of radiogenic Sr from the Cambrian metapelitic host rocks. Metamorphic fluids liberated during magmatism may have carried this strontium into the magma that was undergoing magmatic-hydrothermal evolution at that time. Also, mobility of Rb (together with K, see Fig. 4a)

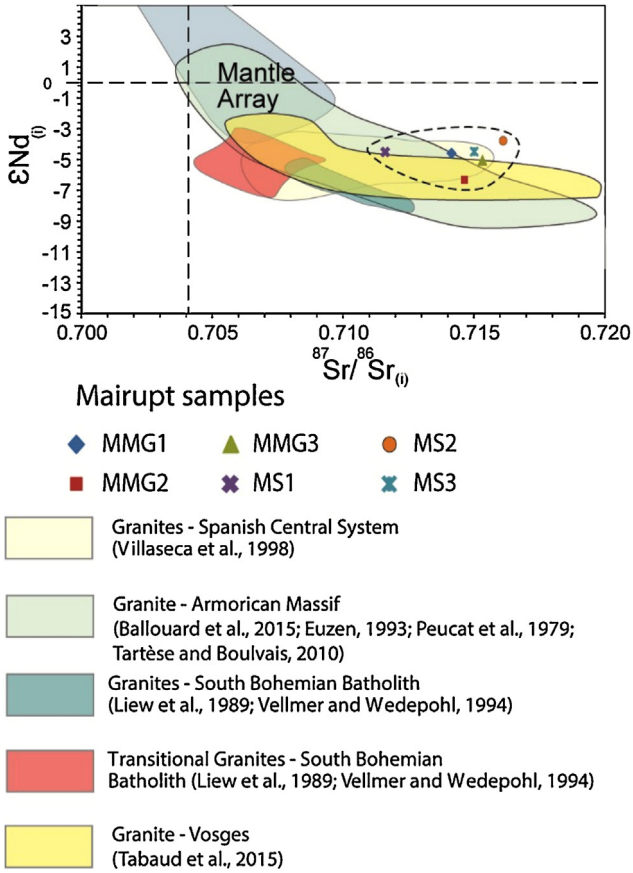

Fig. 6. Sr–Nd isotope diagram for the Mairupt microgranite. The data for the granites from the European Hercynian Belt (Armorican Massif, Spanish Central System, Vosges, and South Bohemian Batholith) are plotted for comparison. Data from our study are surrounded by a black dashed-line. See Euzen, 1993; Peucat et al., 1979; Tabaud et al., 2015; Tartèse and Boulvais, 2010; Villaseca et al., 1998.

during regional deformation and metamorphism associated with the Hercynian shortening tens of millions of years after the microgranite emplacement may have led to disturbance of the Rb–Sr isotopic system, and thus to the observed spreading of Sr initial isotope ratios. It remains that the radiogenic Sr and unradiogenic Nd signatures of the microgranite-($^{87}Sr/^{86}Sr)_i \geq 0.711$ (based on the protolith MS1 sample); $\varepsilon_{Nd(t)} = -4$ to -6 are very likely primary characteristics of the magma itself.

6.2.2. Magmatic source

The chemical and isotopic characteristics of the Mairupt microgranite likely reflect a dominant crustal contribution, as evidenced by:

- the moderate to highly radiogenic Sr isotope composition, with a minimum initial $^{87}Sr/^{86}Sr$ ratios of 0.711;
- the peraluminous signature of the microgranite;
- the Zr/Hf ratio (~44), close to the value of the continental crust (Wedepohl, 1995);
- other features as the enrichment in LREE or the presence of inherited cores in the zircon grains.

In the $\varepsilon_{Nd(t)}$ vs. $^{87}Sr/^{86}Sr_{(i)}$ diagram (Fig. 6), the Mairupt microgranite defines a field close to and overlapping the field of various peraluminous granites emplaced during the Hercynian collision in Europe. The Hercynian granites derived from melts which were formed from lower (or middle) crustal source, with very limited mantle-derived components (Liew et al., 1989; Klötzli et al., 2001; Vellmer and Wedepohl, 1994).

Besides their peraluminous characters and overlapping isotopic compositions, the SCS (Spanish Central System) granites and the Mairupt microgranite share other common geochemical features, such as comparable K/Rb (140–240 for the SCS, 83–245 for Mairupt), La_N/Yb_N (6–13 for the SCS, 1–4 for Mairupt, and Eu/Eu* ratios (0.34–0.62 for the SCS, 0.30–0.64 for Mairupt; see Villaseca and Herreros, 2000 for the SCS values). These features are considered as being inherited from the primary source of the SCS granites (Villaseca and Herreros, 2000). One can therefore suggest that the lower (and/or middle) crust is a likely source for the Mairupt microgranite.

6.3. Geodynamical context at 420 Ma (Upper Silurian/Lower Devonian)

Based on our results, the Mairupt microgranite is similar in age with the volcanites interbedded in Upper Silurian/Lower Devonian strata in the Willerzie area, which

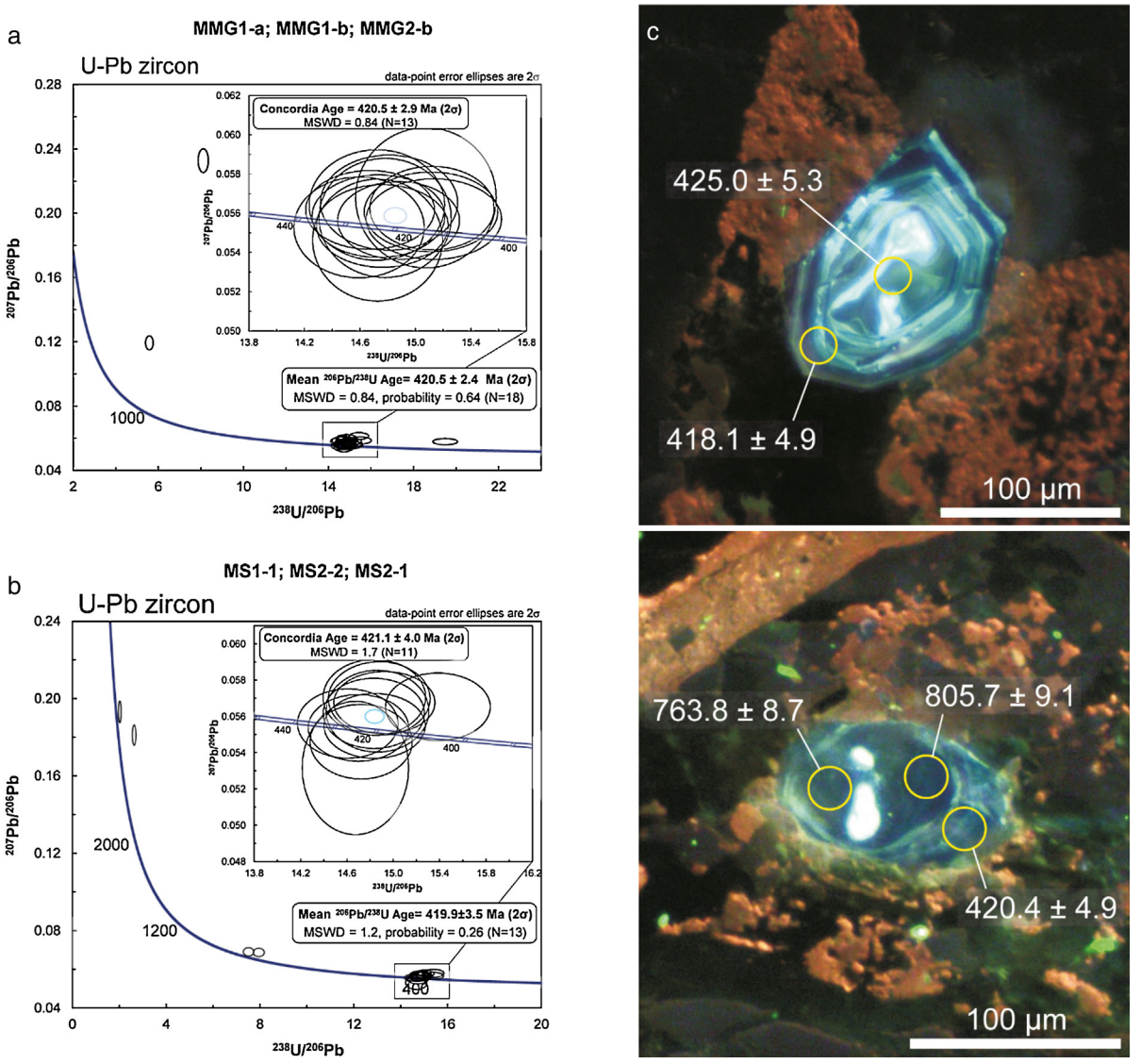

Fig. 7. Tera–Wasserburg diagrams of in-situ zircon analyses in (a) samples MMG1-a, MMG1-b and MMG2-b and (b) MS1-1, MS2-2 and MS2-1. Error ellipses are plotted at 2 σ. (c) Cathodoluminescence micrographs of zircon crystals in the Mairupt microgranite (blue luminescence). The locations of the laser ablation spots and the corresponding $^{206}Pb/^{238}U$ age (in Ma) are shown. The brown-luminescing mineral is albite.

includes rhyolite clasts (Roche et al., 1986) and porphyroid layers (Beugnies, 1969; Corin, 1965). These strata are lying unconformably on the Lower Paleozoic basement and were deposited during the initiation of the Upper Silurian/Devonian transgression, which occurred on the Ardenne (South Avalonia) paleo-margin (Meilliez, 1989, 2006). Therefore, the volcanites of the Willerzie area may be regarded as the effusive expression of the Siluro-Devonian sub-volcanic dykes of the Rocroi inlier. This scenario was already proposed by Beugnies (1969) and Beugnies and Charlet (1970), but subsequently invalidated by Goffette et al. (1991). The magmatic dykes occurring in the nearby Givonne inlier could have the same origin as they crosscut the Variscan unconformity (e.g., Beugnies, 1960; Darimont, 1989). Interestingly, a bimodal magmatism of Late Silurian/Early Devonian age similar to that in the Rocroi inlier is known further to the south in the Hercynian belt, in the so-called Saint-Georges-sur-Loire synclinorium (Ballèvre et al., 2009), even if the geodynamical contexts of the Rocroi area and the Saint-Georges-sur-Loire one are parts of distinct tectonic (sub-)plates.

The Rocroi inlier, and the Ardenne Allochton in general, are parts of the Rheno-Hercynian zone extending along the southern continental margin of Laurussia (Golonka and Gaweda, 2012; Meilliez et al., 1991; Verniers et al., 2002). This zone corresponds to a back-arc basin, associated with north-dipping subduction of the Gondwana plate (Kroner and Romer, 2013; Kroner et al., 2007; Fig. 8). A transtensional setting was already suggested by Goffette (1991) based on structural analysis of the dykes in the Rocroi inlier. We propose that lithospheric stretching in such a transtensional context was responsible for mantle

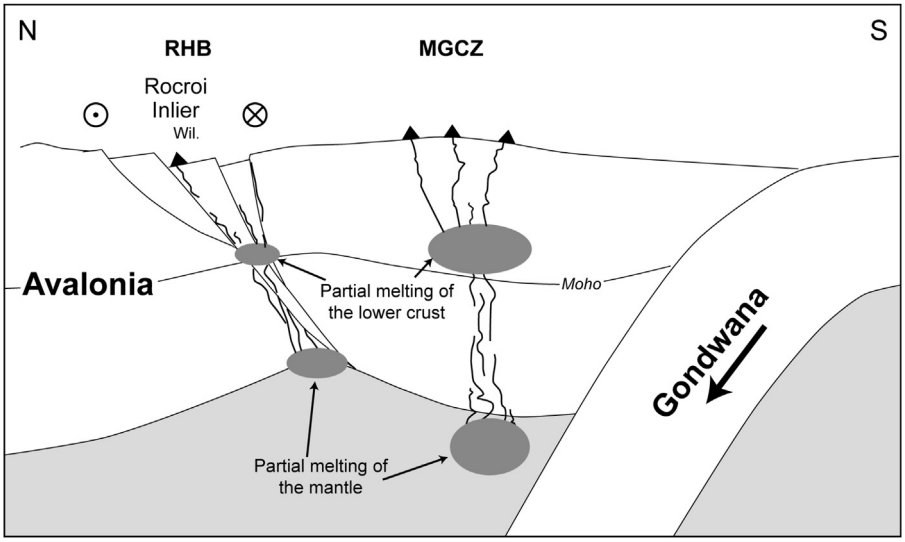

Fig. 8. Schematic representation (not to scale) of the back-arc geodynamical context prevailing at 420 Ma in the Ardenne margin. MGCZ: Mid German Crystalline Zone. RHB: Rheno-Hercynian back-arc Basin (Kroner and Romer, 2013). Wil.: Willerzie volcanites.

decompression and melting. The bimodal magmatism now preserved as diabase and microgranite dykes (including Mairupt) and felsic volcanics may be explained in this context. Tholeiitic mafic magmas were generated in the mantle, and peraluminous granitic magmas by partial melting of the lower crust, the latter being likely triggered by accumulation of mafic rocks at the base of the crust (underplating).

7. Conclusion

Magmatic activity in the Rocroi inlier was dated by zircon U–Pb geochronology using LA–ICP–MS on the Mairupt microgranite. The obtained age is 420.5 ± 2.9 Ma (Late Silurian/Early Devonian), which is ca. 50 Ma older than a previously reported dating of this intrusion. The felsic volcanites interbedded in the Uppermost Silurian/Lowermost Devonian strata from the Willerzie area are thus synchronous and represent the effusive part of the same magmatic system, as previously suggested. Even though the microgranite has been altered to some extent, its geochemical signatures reliably indicate a dominant crustal contribution. We propose that the magmatism in the Rocroi inlier is related to a crust thinning process of the Ardenne margin during the onset of Uppermost Silurian/Lowermost Devonian sedimentation in the transtensional context of the Rheno-Hercynian back-arc basin.

Acknowledgments

The authors want to thank Yann Lepagnot and David Vilbert for their help during rock crushing and Sr and Nd analyses respectively. This research was supported by the Research Institute for Materials Science and Engineering (UMONS).

Appendix A. Supplementary data

Supplementary data associated with this article can be found, in the online version, at https://doi.org/10.1016/j.crte.2017.12.001.

References

André, L., 1983. Origine et évolution des roches éruptives du Massif du Brabant (Belgique). Free University of Brussels, [Unpublished Ph.D thesis]

Ballèvre, M., Bosse, V., Ducassou, C., Pitra, P., 2009. Palaeozoic history of the Armorican Massif: models for the tectonic evolution of the suture zones. C. R. Geoscience 341, 174–201.

Ballouard, C., Boulvais, P., Poujol, M., Gapais, D., Yamato, P., Tartèse, R., Cuney, M., 2015. Tectonic record, magmatic history and hydrothermal alteration in the Hercynian Guérande leucogranite, Armorican Massif, France. Lithos 220, 1–22.

Ballouard, C., Poujol, M., Boulvais, P., Branquet, Y., Tartèse, R., Vigneresse, J.L., 2016. Nb-Ta fractionation in peraluminous granites: a marker of the magmatic-hydrothermal transition. Geology 44 (3), 231–234.

Beugnies, A., 1960. Le massif cambrien de Givonne. Ann. Soc. Geol. Belgique 83, 1–40.

Beugnies, A., 1963. Le massif cambrien de Rocroi. Bull. Serv. Carte geol. France 270, 155.

Beugnies, A., 1968. Livret guide des excursions dans le Massif cambrien de Rocroi, de Fépin à Bovigny suivant la vallée de la Meuse. Soc. belge Geol., Paleont. Hydrol. 1–38 .

Beugnies, A., 1969. Les roches à quartz dihexaédrique du Franc-Bois de Willerzie. Bull. Soc. belge Geol. 68, 311–329.

Beugnies, A., Charlet, J.M., 1970. Sur l'âge hercynien des microgranites du massif cambrien de Rocroi. Ann. Soc. Geol. Belgique 93, 431–452.

Carignan, J., Hild, P., Mevelle, G., Morel, J., Yeghicheyan, D., 2001. Routine analyses of trace elements in geological samples using flow injection and low pressure on-line liquid chromatography coupled to ICP-MS: a study of geochemical reference materials BR, DR-N, UB-N, AN-G and GH. Geostandards Newslet. 25, 187–198.

Corin, F., 1965. Atlas des roches éruptives de Belgique. Mem. Serv. Geol. Belgique 4, 190.

Darimont, A., 1989. Veines de quartz riches en azote dans l'aire métamorphique de Givonne, Belgique. Ann. Soc. Geol. Belgique 112, 151–155.

Euzen, T., 1993. Pétrogenèse des granites de collision post-épaississement : le cas des granites crustaux et mantelliques du complexe de Pontivy-Rostrenen (Massif Armoricain, France). Université Rennes 1.

Evensen, N.M., Hamilton, P.J., O'nions, R.K., 1978. Rare-earth abundances in chondritic meteorites. Geochim. Cosmochim. Acta 42, 1199–1212.
Goffette, O., 1991. Le magmatisme varisque en Ardenne méridionale : un marqueur de l'évolution géodynamique d'une paléomarge. University of Lille, [Ph.D thesis]
Goffette, O., Liégeois, J.-P., André, L., 1991. Age U-Pb sur zircon dévonien moyen à supérieur du magmatisme bimodal du Massif de Rocroi (Ardenne, France): implications géodynamiques. C.R. Acad. Sci. Paris, Ser. II 312, 1155–1161.
Golonka, J., Gaweda, A., 2012. Plate tectonic evolution of the southern margin of Laurussia in the Paleozoic. In: Tectonics – recent advances. [ISBN: 978-953-51-0675-3].
Gosselet, J.A.A., 1888. L'Ardenne. Baudry et Cie, Paris, France.
Grant, J.A., 1986. The isocon diagram; a simple solution to Gresens' equation for metasomatic alteration. Econ. Geol. 81, 1976–1982.
Hughes, C.J., 1973. Spilites, keratophyres, and the igneous spectrum. Geol. Mag. 109, 513–527.
Jackson, S.E., Pearson, N.J., Griffin, W.L., Belousova, E.A., 2004. The application of laser ablation-inductively coupled plasma-mass spectrometry to in situ U–Pb zircon geochronology. Chem. Geol. 211, 47–69.
Klötzli, U.S., Koller, F., Scharbert, S., Höck, V., 2001. Cadomian lower-crustal contributions to Variscan granite petrogenesis (South Bohemian Pluton, Austria): constraints from zircon typology and geochronology, whole-rock, and feldspar Pb–Sr isotope systematics. J. Petrology 42, 1621–1642.
Kroner, U., Hahn, T., Romer, R.L., Linnemann, U., 2007. The Variscan orogeny in the Saxo-Thuringian zone – heterogenous overprint of Cadomian/Paleozoic peri-Gondwana crust. Geol. Soc. Am. Spec. Papers 423, 153–172.
Kroner, U., Romer, R.L., 2013. Two plates – many subduction zones: the Variscan orogeny reconsidered. Gondwana Res. 24, 298–329.
Lacquement, F., 2001. L'Ardenne Varisque: déformation progressive d'un prisme sédimentaire pré-structuré, de l'affleurement au modèle de chaîne, 29Société géologique du Nord, pp. 285, [Ph.D thesis]
Liew, T.C., Finger, F., Höck, V., 1989. The Moldanubian granitoid plutons of Austria: chemical and isotopic studies bearing on their environmental setting. Chemical Geol. 76, 41–55.
Ludwig, K.R., 1998. On the treatment of concordant uranium-lead ages. Geochim. Cosmochim. Acta 62, 665–676.
Ludwig, K.R., 2001. Isoplot/Ex (rev. 2.49), a geochronological toolkit for Microsoft Excel. Berkeley Geochronology Center Special Publication No. 1a, 55. University of California, Berkeley.
Meilliez, F., 1989. Tectonique distensive et sédimentation à la base du Dévonien, en bordure NE du massif de Rocroi (Ardenne). Ann. Soc. Geol. Nord 107, 281–295.
Meilliez, F., 2006. La discordance éodévonienne de l'Ardenne : caractérisation stratigraphique et paléo-environnementale de la Formation de Fépin et ses conséquences. Geol. Fr. 1–2 .
Meilliez, F., André, L., Blieck, A., Fielitz, W., Goffette, O., Hance, L., Khatir, A., Mansy, J., Overlau, P., Verniers, J., 1991. Ardenne-Brabant. Sci. Geol. Bull. 44, 3–29.
Peucat, J.-J., Charlot, R., Mifdal, A., Chantraine, J., Autran, A., 1979. Définition géochronologique de la phase bretonne en Bretagne centrale. Étude Rb/Sr de granites du domaine centre-armoricain. Bull. BRGM 1, 349–356.
Roche, M., Sabir, M., Steemans, P., Vanguestaine, M., 1986. Palynologie de la région et du sondage de Willerzie. Aardkundige Mededelingen 3, 149–190.
Sláma, J., Košler, J., Condon, D.J., Crowley, J.L., Gerdes, A., Hanchar, J.M., Horstwood, M.S., Morris, G.A., Nasdala, L., Norberg, N., 200. Plesovice zircon – a new natural reference material for U–Pb and Hf isotopic microanalysis. Chemical Geol. 249, 1–35.
Sun, S.-S., 1980. Lead isotopic study of young volcanic rocks from mid-ocean ridges, ocean islands and island arcs. Philos. Transact. Royal Soc. London A: Math. Phys. Eng. Sci. 297, 409–445.
Tabaud, A.-S., Janoušek, V., Skrzypek, E., Schulmann, K., Rossi, P., Whitechurch, H., Guerrot, C., Paquette, J.-L., 2015. Chronology, petrogenesis and heat sources for successive Carboniferous magmatic events in the Southern-Central Variscan Vosges Mts (NE France). J. Geol. Soc. 172, 87–102.
Tartèse, R., Boulvais, P., 2010. Differentiation of peraluminous leucogranites "en route" to the surface. Lithos 114, 353–368.
Van Achterbergh, E., Ryan, C.G., Jackson, S.E., Griffin, W.L., 2001. Data reduction software for LA-ICPMS: appendix. Laser Ablation-ICP Mass Spectrometry in the Earth Sciences: principles and applications (P.J. Sylvester, ed.). Mineral. Assoc. Canada 29, 239–243.
Vellmer, C., Wedepohl, K.H., 1994. Geochemical characterization and origin of granitoids from the South Bohemian Batholith in Lower Austria. Contrib. Mineral. Petrol. 118, 13–32.
Verniers, J., Pharaoh, T., André, L., Debacker, T.N., De Vos, W., Everaerts, M., Herbosch, A., Samuelsson, J., Sintubin, M., Vecoli, M., 2002. The Cambrian to mid-Devonian basin development and deformation history of eastern Avalonia, east of the Midlands Microcraton: new data and a review. Geol. Soc. London 201, 47–93.
Villaseca, C., Barbero, L., Rogers, G., 1998. Crustal origin of Hercynian peraluminous granitic batholiths of central Spain: petrological, geochemical and isotopic (Sr, Nd) constraints. Lithos 43, 55–79.
Villaseca, C., Herreros, V., 2000. A sustained felsic magmatic system: the Hercynian granitic batholith of the Spanish Central System. Trans. Roy. Soc. Edinburgh: Earth Sci. 91, 207–219.
Wedepohl, K.H., 1995. The composition of the continental crust. Geochim. Cosmochim. Acta 59, 1217–1232.